MRI visualization of neuroinflammation using VCAM-1 targeted paramagnetic micelles.

Garello F, Pagoto A, Arena F, Buffo A, Blasi F, Alberti D, Terreno E.

Published in Nanomedicine

doi: 10.1016/j.nano.2017.10.002

Available online 1 November 2017

MRI visualization of neuroinflammation using VCAM-1 targeted paramagnetic micelles

Francesca Garello,[1] Amerigo Pagoto,[1] Francesca Arena,[1] Annalisa Buffo,[2,3] Francesco Blasi,[1] Diego Alberti,[1] and Enzo Terreno[1*]

[1] Molecular & Preclinical Imaging Centers, Department of Molecular Biotechnology and Health Sciences, University of Torino, Via Nizza 52, 10126 Torino, Italy

[2] Department of Neuroscience Rita Levi-Montalcini, University of Turin, 10126 Turin, Italy

[3] Neuroscience Institute Cavalieri Ottolenghi, Regione Gonzole 10, 10043 Orbassano, Turin, Italy

[*]*Prof. Enzo Terreno. Molecular & Preclinical Centers, Department of Molecular Biotechnology & Health Sciences, University of Torino. Address: Via Nizza 52, 10126 – Torino, Italy*

Phone: +39-011-6706452 Fax: +39-011-6706487 e-mail: enzo.terreno@unito.it

Word count

Abstract: 145 words

Complete manuscript: 5044 words

Number of references: 58

Number of figures and/or tables: 8

European Union's FP7/2007–2013 under grant agreement no. HEALTH-F2-2011-278850 (INMiND) and Fondazione Umberto Veronesi "FUV" are gratefully acknowledged. The authors declare that there is no conflict of interest regarding the publication of this article.

Abstract

The detection of neuroinflammatory processes using innovative and non-invasive imaging techniques is of great help to deeply investigate the onset and progression of neurodegenerative diseases. Since Vascular Cell Adhesion Molecule (VCAM-1) is over expressed at the blood brain barrier in the event of neuroinflammation, the goal of this work was the testing of MRI detectable micelles targeted towards VCAM-1 to visualize inflamed regions in a mouse model of acute neuroinflammation. The developed probe allowed for the early detection of the disease, with higher T_1 signal enhancement and more precise localization in comparison to untargeted micelles or to the clinically approved contrast agent MultiHance. Moreover, the relatively long blood half-life of the nanosystem (*ca.* 6.3 h) guaranteed a good accumulation in the inflamed regions, paving the way to future diagnostic/theranostic applications, implying the loading of neuroprotective or even anti-cancer drugs inside the core of the micelles.

Keywords

VCAM-1; MRI; Gd-complexes; micelles; neuroinflammation.

Introduction

Neuroinflammation is an active multifaceted adaptive process. It has been detected in infectious brain diseases as well as following central nervous system (CNS) traumatic injury, and, more recently, in patients affected by various neurodegenerative pathologies.[1-3] The main features of this dynamic process are: (i) changes in the vasculature, (ii) activation of resident immune competent cells, (iii) infiltration of blood circulating immune cells (neutrophils, macrophages, lymphocytes), and (iv) cytokine production.[4,5] This orchestrated machinery would have the purpose of limiting the extent of the disease, clearing tissue damage and supporting repair and regeneration; but at the same time, it could lead to the boosting and perpetuation of inflammation.[6-8] The precise mechanisms regulating and driving this frail equilibrium are not completely clarified yet. Indeed, the close relationship between neuroinflammation and the onset and development of many neurodegenerative diseases is becoming more and more undeniable.[9-15] Since these disorders are affecting millions of people worldwide and their prevalence is expected to raise in the next decades,[5] the need for specialized non-invasive imaging techniques is increasing to better clarify the role and the spatio-temporal correlation between inflammation and degeneration. So far, in clinics, most of the available imaging techniques allowed for the diagnosis of neurodegenerative diseases only at later stage of progression, hence limiting the treatment outcome.[16-18] Various targeted Positron Emission Tomography (PET) tracers have been designed and tested in clinics to detect neurodegeneration or neuroinflammation.[19-21] However, despite the great sensitivity of PET imaging and the possibility to obtain quantitative information, these compounds, due to their lipophilic nature, display a considerable non-specific binding, resulting in remarkable signal overlap with control patients.[22-25] In addition, PET imaging is characterized by high costs, reduced half-life time of the tracers and limited follow up of the patients due to the invasiveness of the technique. A valuable alternative to PET is Magnetic Resonance Imaging (MRI), which with its outstanding spatial resolution, moderate cost-effectiveness, relatively slow kinetics of probes and lack of radiation exposure, can be considered a technique of choice in

neuroimaging. The diagnosis of different neurological disorders, indeed, can be performed through the MR assessment of volume changes in specific brain regions or the MR detection of distinct pathological hallmarks.[26-31] However, routine structural neuroimaging evaluations are normally based on the observation of late features in the progression of the disease. Therefore, the development of new MRI approaches for early and specific recognition of neurological diseases at the prodromal stages would be of crucial importance. In light of the low sensitivity of MRI and of the difficulties encountered by the mostly hydrophilic paramagnetic probes in overcoming an intact blood brain barrier (BBB), a suitable strategy to obtain a considerable signal is the development of molecules targeting the neuroinflammation-mediated changes in the vasculature. More in details, in the event of neuroinflammation, infiltration of immune cells from the bloodstream into CNS parenchyma occurs through a sequential and coordinated process involving tethering, rolling, adhesion and transmigration of leucocytes across the BBB.[32,33] Each step involves interaction of BBB endothelial cells and leukocytes via endothelial expression of Cell Adhesion Molecules (CAMs), among which vascular CAM-1 (VCAM-1) is one of the most investigated. VCAM-1 is not constitutively expressed on the endothelium but is up-regulated upon endothelial activation, thus being an attractive target of early cerebral inflammation, easily accessible to blood borne contrast agents.[34-36] Superparamagnetic iron oxide microparticles (MPIO) were already conjugated to antibodies[37-38] or peptidic vectors[39] for targeting VCAM-1 receptors to generate highly specific hypointense contrast effects associated with the overexpression of the target in animal models where inflammation is relevant. However, so far, Gd-containing nanosystems targeting the over expression of VCAM-1 have not been tested yet in the visualization of CNS inflammation.[40] Indeed, the use of positive contrast agents is advisable to unequivocally locate the inflamed region, avoiding signal misunderstandings due to the presence of haemorrhages, air or abnormal mineral substances accumulation.[41] In addition, as MPIO are avidly taken up from the immune system cells, the use of stealthier particles is desirable to increase the blood half-life time of the system and increase the targeting selectivity. In the herein reported work, VCAM-1 targeted Gd-based paramagnetic micelles, developed by our group and already successfully

validated on a model of peripheral inflammation,[42] were tested in a murine model of acute neuroinflammation to investigate their potential application in the early detection of neurodegenerative processes.

Methods

1.1 Materials

See Supplementary Information.

1.2 Animal Care and Use

C57BL/6J female mice (8-12 weeks old) were obtained from the animal facility at the Molecular Biotechnology Center of the University of Torino. The animal study was approved by the Italian Ministry of Health; the procedures followed were in accordance with institutional guidelines and ensured the humane care of the animals. Anaesthesia was provided by 1-2 % isoflurane inhalation or by intramuscular injection of a combination of 20 mg/kg tiletamine/zolazepam (Zoletil 100; Virbac, Milan, Italy) and 5 mg/kg xylazine (Rompun; Bayer, Milan, Italy).

1.3 Micelles Preparation and Characterization

The synthesis of the VCAM-1 targeted peptide (C*NNSKSHTC*) or of its scrambled version (HSC*NKNSC*T) was carried out as described elsewhere.[42] The peptides were then cyclized and conjugated to the phospholipid DSPE-PEG2000-NH_2 to obtain the DSPE-PEG2000-VCAM1-peptide (Figure S1) or the DSPE-PEG2000-scrambled-peptide, respectively.

VCAM-1 targeted micelles were prepared through the lipid film hydration method, followed by sonication, using the following composition: DSPE-PEG2000, Gd-DOTAMA$(C18)_2$, DSPE-PEG2000-peptide (targeted or scrambled) and Rhodamine-DOPE in a molar ratio of 57.5:40:2:0.5, with a final lipid concentration of 15 mg/mL. The suspension was sonicated twice for 90 s (power 50

W, Sonicator Bandelin Sonoplus HD 2070, Berlin, Germany). During sonication, the mixture was cooled with ice to keep the temperature under 10 °C. The mean hydrodynamic diameter and polydispersity index (PDI) were determined by Dynamic Light Scattering (DLS) (Malvern, Zetasizer) 30 min after preparation. The millimolar longitudinal relaxivity (r_1) of the paramagnetic nanoparticles was measured at 0.5 T (Stelar Spinmaster Spectrometer, Pavia, Italy). The concentration of Gd(III) in the micelle suspension was determined relaxometrically.[43]

1.4 Estimation of VCAM-1 receptor expression

The expression of VCAM-1 receptor in bEnd.3 cells before and after activation with Tumor Necrosis Factor alpha (TNF-alpha) was determined as reported in the Supporting Information.

1.5 In vitro assays

An *in vitro* assay was performed to evaluate the binding ability of targeted micelles to VCAM-1 receptors in brain endothelial cells (see Supporting Information).

1.6 Half-life time of VCAM-1 targeted micelles

The blood half-life time of VCAM-1 targeted micelles was investigated in healthy C57BL/6J female mice (n=3). Micelles were administered through tail vein injection at 0.05 $mmol_{Gd}$/kg body weight. At different time points (5, 15, 30 min, 1, 2, 4 and 24 h) post injection, a micro aliquot of blood was collected from the tail vein. 20 μL of Heparin (500 UI/mL) were added to each sample to avoid coagulation. The volume of blood collected at each time was quantified, then the samples were digested with concentrated HNO_3 (70%, 1 mL) under microwave heating, recollected in ultrapure milli-Q water and analyzed by ICP-MS to measure Gd(III) content at each time point. Data obtained,

displayed as millimolar concentration *vs.* time post injection, were fitted with a mono-exponential decay curve and the half-life time was calculated.

1.7 LPS-induced neuroinflammation model

Acute neuroinflammatory response was induced in the right striatum of 8 to 12-week-old C57BL/6J female mice (weight 18±3 g). See Supporting Information for further details.

1.8 In vivo MRI

All the MR images were acquired on a Bruker Icon (1 T) equipped with a brain surface coil. Animals were recruited 24 hours post LPS injection. MRI acquisition was performed under 1 % isoflurane anaesthesia. Animals were scanned before and 20 min, 4 h, 24 h, 48 h post injection of VCAM-1 targeted paramagnetic micelles or micelles decorated with the scrambled peptide. T_2-weighted MRI images were obtained using a RARE sequence protocol (TR/TE/NAV=2500/26.7/12). T_1-weighted MRI images were acquired using a FLASH sequence (TR/TE/NAV = 75/5.8/18, field of view (FOV) = 1.2 cm). To compare the contrast obtained with VCAM-1 targeted micelles with the one obtained after the administration of the clinically approved contrast agent MultiHance^{TM}, the agent was injected in the tail vein, 24 hours after the induction of inflammation, at the concentration of 0.2 mmol Gd/kg and the animals were imaged repeatedly for 30 minutes.

1.9 Image processing and analysis

Image analysis was performed using Bruker ParaVision 5.1 imaging software. Regions of interest (ROIs) were drawn over right (inflamed) and left (non-inflamed) striatum in the imaging plan and average signal intensity was measured. The % T_1 signal enhancement (% T_1-SE) over pre-images was calculated as follows:

$$\%\ T_1\ SE = \frac{SNR_t - SNR_0}{SNR_0}\ x\ 100$$

where

$$SNR_i = \frac{SI_i}{SD_i\ noise}$$

SNR stands for Signal to Noise Ratio, SI stands for Signal Intensity (with *i* = 0 or *t*), while *0* and *t* refer to the measurement carried out before and after the injection of the contrast agent, respectively.

1.10 Biodistribution of VCAM-1 targeted micelles

Micelle homing to the main excretory organs, liver, kidneys and spleen, was followed by MRI at different time points after the administration of VCAM-1 targeted micelles (*n*=6). 24 hours post injection the animals were sacrificed and the liver, spleen, kidneys, lungs, left and right cerebral hemispheres were excised, weighted and digested in concentrated nitric acid (70%) under microwave heating, recollected in ultrapure milli-Q water and analyzed by ICP-MS to measure Gd content. The amount of Gd (mg_{Gd}/g_{organ}) was calculated. Moreover, an estimation of the percentage of residual Gd in each organ according to the administered dose was evaluated in all the excised organs as follows:

$$\%\ Gd = \frac{mol\ Gd_{g\ organ}\ x\ g\ organ}{mol\ Gd\ administered}\ x\ 100$$

1.11 Ex-vivo studies

To investigate the presence of VCAM-1 targeted micelles in the inflamed brain regions, 24 hours post administration of the nanosystem the animals (*n*=2) were sacrificed following MRI acquisition and the brain was extracted and cryopreserved for immunofluorescence studies (see Supporting Information).

1.12 Statistical analysis

All data were presented as mean values ± Standard Error of mean (SE). Significant differences among experimental conditions were identified by applying the one-way ANOVA test, assuming statistical significance at $p < 0.05$.

Results

3.1 Micelle Preparation and Characterization

VCAM-1 targeted paramagnetic micelles were prepared by the lipid thin film hydration method. The mean size of the obtained nanosystem, checked by DLS, was 17 ± 2 nm with a PDI value of 0.2 ± 0.1 (13 replicates). The longitudinal relaxivity (r_1) measured at 1 T and 37°C was 35.0 $s^{-1}mM_{Gd}^{-1}$. Micelles bearing the scrambled version of the targeting peptide did not differ significantly in size and relaxivity in comparison to the VCAM-1 directed nanosystem.

3.2 Estimation of VCAM-1 receptor expression

In order to investigate the BBB targeting of the developed micelles, the murine brain endothelial cell line bEnd.3 was chosen as *in vitro* model**.** Although these cells are reported to constitutively express VCAM-1 receptor below passage 30, stimulation with TNF-alpha further increases the receptor expression. Flow cytometry was employed to investigate the presence of the surface receptor before and 4 h after incubation with TNF-alpha. The analysis of cell samples acquired by fluorescence-activated cell sorting (FACS) after incubation with the FITC anti VCAM-1 antibody showed a remarkable enhancement in VCAM-1 expression after treatment with TNF-alpha. (Figure S2)

The mean number of VCAM-1 receptors/cell was determined by spectrofluorimetry. More in details, before and after treatment with TNF-alpha, the cells were incubated with FITC-tagged anti VCAM-1 antibody to label the receptor. Subsequently, the cells were washed and sonicated in order to

measure for each sample the mg of proteins, correlated to the number of cells, and the fluorescence intensity, correlated to the number of receptors. The results obtained displayed a four-fold increase in VCAM-1 expression after treatment with TNF-alpha (Figure 1), thus validating the use of such brain endothelial cells as *in vitro* model to assess the potential interaction between the receptor and the targeted nanosystem.

3.3 In vitro targeting assays

The affinity of targeted and non-targeted micelles towards VCAM-1 receptors was investigated *in vitro* using bEnd.3 cells. The whole experiment was carried out at 4°C in order to avoid the cell internalization of the nanosystem. Confocal microscopy images, taken 30 min after incubation with the targeted micelles, proved that the selected timeframe was sufficient to achieve a considerable cell membrane labeling (Figure S3). An overall enhancement in the red fluorescence from naïve to activated bEnd.3 cells was observed, suggesting the presence of an active membrane labeling process.

To quantify the amount of receptor-bound nanosystem and the MRI signal obtained after incubation of cell samples with targeted or scrambled micelles, an additional experiment was performed. More in detail, cells were detached with EDTA before and after treatment with TNF-alpha; incubation with targeted or untargeted (*i.e.* conjugated with a scrambled peptide) micelles (total Gd(III) concentration 2 mM) was performed in suspension for 30 min at 4°C. At the end of the incubation, cells were profusely washed to remove unbound micelles, and then centrifuged into glass capillaries to obtain a cell pellet. The pellet was imaged by MRI at 7.0 Tesla and the T_1 of each sample was measured. Immediately after imaging, the cell pellets were recollected and sonicated to estimate the number of bEnd.3 cells using the Bradford assay and to quantify the amount of gadolinium by ICP-MS.

The amount of Gd(III) found in activated cells incubated with targeted micelles was *ca.* 90 % higher than cells incubated with scrambled micelles (1.5×10^{-15} *vs.* 7.9×10^{-16} mol_{Gd}/cell). A similar disparity was noticed between the amount of Gd(III) in activated and non-activated cells incubated with VCAM-1 targeted micelles (1.5×10^{-15} *vs.* 6.6×10^{-16} mol_{Gd}/cell, $p<0.05$) (Figure 2A). No significant

differences were found in non activated cells incubated with VCAM-1 targeted or untargeted micelles. Interestingly, the relaxivity values determined for the non activated cells were slightly lower than the activated ones, and, for the latter, the relaxivity of the targeted micelles was higher than the untargeted nanosytem (Figure 2B). The combination between the amount of cell-bound Gd and the relaxivity value justifies the different MRI contrast observed in the pellets (Figure 2C), where the samples incubated with VCAM-1 targeted micelles displayed the higher contrast.

3.4 In vivo blood half-life time of VCAM-1 targeted micelles

The blood half-life time of VCAM-1 targeted micelles was assessed in healthy mice (n=3). The targeting nanosystem was administered by tail vein injection, and blood samples were collected at different time points, ranging from 5 min to 24 hours, mixed with heparin to avoid coagulation, and quantified in terms of volume. Following digestion in concentrated nitric acid, the exact amount of Gd(III) at each time point was determined by ICP-MS. Data obtained were plotted and fitted with a mono-exponential decay curve, resulting in a mean half-life time of 376 ± 22 min (R^2= 0.99, Figure 3).

3.5 In vivo MRI

On the basis of the promising *in vitro* results, the potential of VCAM-1 targeted micelles to bind VCAM-1 receptors at the blood brain barrier was investigated in a murine model of neuroinflammation. Acute neuroinflammatory response was induced in the right striatum by local injection of lipopolysaccharide (LPS). The presence of inflammation and the over-expression of VCAM-1 in the involved hemisphere were detectable already 24 hours after surgery by *ex-vivo* histological studies (Figure S4). In the contra-lateral hemisphere, almost no hallmarks of inflammation were present. The animals were enrolled in the study 24 hours after LPS injection, received intravenous administration of VCAM-1 targeted micelles (0.05 mmol Gd/kg body weight)

and were imaged at 1.0 T at 20 min, 4 h, 24 h and 48 h post injection (Figure 4) to monitor micelle homing to the site of inflammation.

In T_{2w} anatomical images, a confined bright area in the inflamed hemisphere was occasionally observed, suggesting the presence of an edematous region. However, only after the injection of VCAM-1 targeted micelles the real extension of the inflamed area was clearly detectable and delineated (Figure 4E). In particular, the T_1 signal enhancement calculated over pre-images, reached a peak value 24 hours post micelle injection, with a statistically significant difference between diseased and healthy hemispheres (39.3 ± 4.4 *vs.* 4.1 ± 2.7 %, respectively, $p < 0.001$, Figure 5).

To ascertain the specificity of the administered nanosystem, a comparison with micelles bearing the untargeted scrambled peptide was conducted. The results obtained displayed a statistically significant difference in the % T_1-SE of the inflamed striatum between targeted and non-targeted micelles at 24 h *p.i.* (39.3 ± 4.4 *vs.* 18.9 ± 2.2 %, respectively, ANOVA *p-values* = 0.003, Figure 6). At the other time points, no statistically significant differences between the two nanosystems were detected (see supporting information, Figure S5-S6).

Interestingly, the kinetic of the contrast enhancement observed for the two nanosystems was a bit different, with the targeted system that performed much better after 24 h post-injection, whereas at 48 h the two micelles showed a very similar effect. Most likely, this observation is an indirect demonstration of the effective targeting of the VCAM-1 directed system, and it suggests that the targeting to the receptor (though, likely, it is not the only process accounting for the accumulation of the probe in the inflamed area) is a faster event than the passive accumulation occurring for the untargeted micelles.

The signal obtained 24 h post injection of the scrambled micelles was definitely comparable to the T_1-SE detected at the same time point after the administration of the contrast agent MultiHance (13.4 ± 2.7 %), which is clinically employed to evaluate the presence of alterations in blood brain barrier permeability. This finding suggests that the contrast obtained after the administration of scrambled

micelles is mainly related to passive extravasation, thus further supporting the view that VCAM-1 targeted micelles effectively bind the corresponding target *in vivo*.

3.6 Biodistribution of VCAM-1 targeted micelles

The biodistribution of the targeted micelles was investigated in the main excretory organs, either *in vivo* by MRI (at 20 min, 4 h and 24 h post injection) or *ex-vivo* by ICP-MS (Gd quantification at 24 h post injection, see Supporting Information). Moreover, with the prospect of assessing the real power of the targeted nanomedicine, the percentage of the metal found in the main excretory and targeted organs 24 hours post injection was calculated over the total administered Gd(III) dose. As displayed in Figure 7, the large majority of the administered Gd(III) (44 ± 5%) accumulated in the liver, whereas much less Gd (0.5-3 %) was found in spleen, lungs, and kidneys. Though only a very small fraction was found in the inflamed region, the amount accumulated in the LPS-treated hemisphere was 400% higher than healthy contralateral brain (0.29 ± 0.03% *vs.* 0.06 ± 0.01%, respectively, Figure S9; $p < 0.0001$).

3.7 Ex-vivo studies

The effective targeting of VCAM-1 micelles was also investigated *post-mortem* by fluorescence microscopy. Brain slices were obtained from treated mice sacrificed 24 h post injection of targeted micelles. A widespread signal originating from the rhodamine dye embedded in the micelles was detected in the inflamed striatum, whereas only a faint and almost negligible fluorescence was visible in the contra-lateral one (see Supporting Information). Staining of vessels was performed with either anti-CD31 antibody, widely used as marker of brain endothelial cells[44] (Figure 8A), or anti VCAM-1 antibody (Figures 8B-8C). Results obtained showed a massive accumulation of micelles not only stuck to the vessels, but also in the cytoplasm of adjacent and extravasating cells. Remarkably, a high degree of binding to the target was still present 24 h post injection, confirming the peptide targeting efficiency and supporting the idea of employing ultra-small and long circulating nanosystem. As a result of confocal microscopy experiments, the idea that the homing of VCAM-1 targeted micelles at

the inflammation site could be additionally supported by immune system cells was conceived. The hypothesis was based on the view that a variable amount of micelles could be phagocytosed by bone marrow-derived (BMD) cells or activated microglia either during systemic circulation or after the eventual blood brain barrier extravasation. To better clarify this point, brain slices were stained with anti F4-80 antibody (Figures 8D-E) proving a massive presence of macrophages at the lesion site, some of which loaded with the fluorescent micelles. However, sporadic presence of micelles in non-macrophagic cells was still visible. In the brain slices extracted from mice injected with the scrambled nanosystem, instead, fewer micelles were detected and most of them were confined in the cytoplasm of F4-80 positive cells (see Supporting Information, Figure S11). The absence of a widespread number of micelles stacked to the vessels support the idea of an increase of MRI signal closely related to passive extravasation and immune system cell mediated delivery.

Discussion

The development of an imaging probe for the MRI early visualization of neuroinflammation could be of great help in the comprehension, interception and prevention of various neurological disorders. This process, in fact, is diffuse and actively involved in demyelinating and neurodegenerative diseases, stroke and malignant CNS tumors.[45] As extensively reviewed by Pulli *et al.*,[46] VCAM-1 has been selected as target to detect neuroinflammation, mainly by MRI, in manifold papers. However, most of the probes reported were intended to achieve a negative MRI contrast. For instance, 1 μm sized particles of iron oxide conjugated to anti-VCAM1-antibody, further referred to as VCAM1-MPIO, were successfully tested in a model of acute neuroinflammation, of autoimmune encephalomyelitis (EAE) or for earlier detection of brain metastases.[37,47-48] However T_2 contrast agents, despite their great sensitivity, are not ideal to detect subtle neurodegenerative disorders as T_2 hyper-intensities in the brain could be also associated with the presence of haemorrhagic foci, intracranial metastases, mucous- or protein-containing lesions, iron, copper or calcium deposition, turbulent flow of the cerebrospinal fluid, air-containing spaces, demyelination or axonal loss.[41] The

signal obtained with T_1 contrast agents, instead, is more specific and limited to the diseased area, without the occurrence of "blooming artefacts". Actually, Gd-complexes are widely used in clinics to highlight BBB breakdown, but a micromolar accumulation of the probe is required to clearly visualize a signal, thus restricting the detection of inflammation to severe clinical cases and reducing the chances of visualization of mild and early-stage phenomena. So far, the use of targeted T_1 probes has been quite limited in literature, possibly due to the lower sensitivity associated with Gd(III) compounds in comparison to iron oxide particles. Chen *et al.* developed a myeloperoxidase (MPO)-activatable paramagnetic sensor to detect more and confirm smaller and earlier active demyelinating lesions in the EAE model, due to the achievement of longitudinal relaxivity values around 25.0 $mM_{Gd}^{-1}s^{-1}$ (at 1.5 T) in the presence of high amounts of the soluble MPO enzyme.[49] The micellar probe herein presented has the advantage of carrying a quite high payload of Gd(III) chelates per micelle (*ca.* 850, as calculated from the surface area of the micelle components),[42] and it is characterized by a considerably high longitudinal relaxivity value per millimolar concentration of particle of *ca.* 3.0×10^4 $mM^{-1}s^{-1}$ (at 1 T).

The targeted micelles displayed a good *in vitro* affinity towards the brain endothelial cell model investigated (bEnd.3), whose VCAM-1 expression was further increased by TNF-alpha activation.

The *in vivo* T_1 signal enhancement in the inflamed brain measured 24 hours post micelle injection attested at around 40 %, a significant value if considered that it was calculated over the entire striatum. Moreover, the real extension of inflammation visible after the administration of the nanosystem was considerably higher than the one perceived using mere T_2 pre-contrast acquisitions or T_1 images after the injection of the clinical agent MultiHance, thus confirming the good potential of the developed system. The peak of T_1 SE at 24 hours post injection was actually quite unexpected as in our previous work[42] on a peripheral inflammation model, the maximum contrast was detected 4 h post-injection. However, this finding is not unprecedented.[50-52] The reason of this delayed enhancement probably lies in the need of a consistent accumulation of the nanosystem at the lesion site, achievable through

its progressive binding to VCAM-1 receptor, BBB crossing, possible interaction with proteins and labeling of immune cells that conceivably migrate to the CNS.

A deep pharmacokinetic investigation of the nanosystem was performed and resulted in a mean blood-half-life of targeted micelles a bit longer than 6 hours, a value in line with other PEGylated nanosystems[53] and remarkably different to the very short (< 5 min) circulation time reported for the micron-sized anti VCAM-1 iron oxide particles mentioned above.[48] The extended blood circulation time is likely due to the relatively small size of the particle that reduces the recognition by monocytes and macrophages. This is an important finding, not only because a long circulation time may favour the binding of the peptide to the endothelial marker of inflammation, but also for promoting a possible extravasation of the system. As further proof of this observation, the *ex-vivo* histological studies carried out demonstrated the occurrence of a strong binding between micelles and blood brain barrier capillaries, still 24 hours post injection, giving the opportunity to follow VCAM-1 expression for a prolonged time window. Even if the presence of micelles inside microglia/macrophages was detected by confocal microscopy, it has to be still clarified whether the uptake occurred during circulation or directly at the inflammation site. However, as far as the detection sensitivity is concerned, this finding is not disturbing because macrophage infiltration and local microglia activation play a key role in neuroinflammation, and both contribute to enhance the MRI contrast in the diseased site with respect to healthy brain. In spite of the good contrast observed, we found that just the 0.3% of the injected Gd(III) reached the targeting site, against a still remarkable liver accumulation (45 % of the injected metal), attributable to the unspecific sequestering operated by liver-resident macrophages.[54] In principle, several routes can be envisaged to improve the overall performance of the protocol including the modulation of the nanoparticle size, the optimization of the micelle formulation (relative ratio among phospholipids, Gd(III), and targeting peptide), the design of a more efficient Gd(III) chelate, and the development of strategies to reduce the liver accumulation of the nanosystem as the pre-saturation of the resident macrophages through the administration of free-Gd micelles before the injection of the smart nanosystem.[55] The use of micelles is certainly a valuable approach even in view

of the possible exploitation of the VCAM-1 targeted agent for theranostics purposes, as a growing number of papers already demonstrated the advantages of using micelles as drug delivery systems.[56-58] Loading VCAM1-directed micelles with anti-inflammatory or anti-cancer molecules would allow the monitoring and treatment of neuro-inflammatory disorders or CNS malignant cancer, respectively. However, it has to be noticed that effective potential of the presented nano-agent for assessing neuroinflammation in neurodegenerative diseases will require the validation in more clinically relevant models, *i.e.* characterized by a chronic evolution of the pathology.

In summary, this work demonstrates that paramagnetic Gd-loaded targeted micelles have the potential to visualize VCAM-1 expression *in vivo* in a mouse model of acute neuroinflammation. The developed micelles displayed a quite long blood half-life that guarantees a good accumulation in the inflamed region and a well-detectable imaging contrast. Besides the expected vascular target and limited passive extravasation of the micelles, data also suggested an immune-mediated brain accumulation across the BBB of the nanoparticles. Such results could pave the way to interesting future diagnostic/theranostic applications of this nanosystem implying the loading of neuroprotective or even anti-cancer drugs inside the hydrophobic core of the micelles.

Electronic Supporting Information (ESI)

Supporting Information available.

List of abbreviations

BBB Blood Brain Barrier

BMD Bone Marrow-Derived

CNS Central Nervous System

DLS Dynamic Light Scattering

EAE Autoimmune Encephalomyelitis

FACS Fluorescence-Activated Cell Sorting

FOV Field of View

ICP-MS Inductively Coupled Plasma Mass Spectrometry

LPS Lipopolysaccharide

MPIO Microparticles of Iron Oxide

MPO Myeloperoxidase

MRI Magnetic Resonance Imaging

NAV Number of Averages

PBS Phosphate-buffered saline

PDI Polydispersity Index

PET Positron Emission Tomography

RF Rare Factor

Rhodamine-DOPE 1,2-dioleoyl-sn-glycero-3-phosphoethanolamine-N-(lissamine rhodamine B sulfonyl) (ammonium salt)

ROI Regions of Interest

SE Signal Enhancement

$T1_w$ T_1 weighted

$T2_w$ T_2 weighted

TE Echo Time

TNF-alpha Tumor Necrosis Factor alpha

TR Repetition Time

VCAM-1 Vascular Cell Adhesion Molecule

Figure Legends

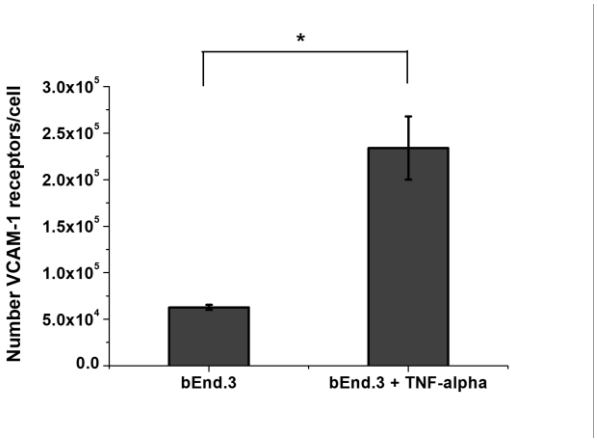

Figure 1. Mean number of VCAM-1 receptors/bEnd.3 cell before and after stimulation with TNF-alpha. The number of cells was estimated with the Bradford assay, while FITC concentration was determined by spectrofluorimetry (* $p < 0.05$). Error bars represent SE of the mean.

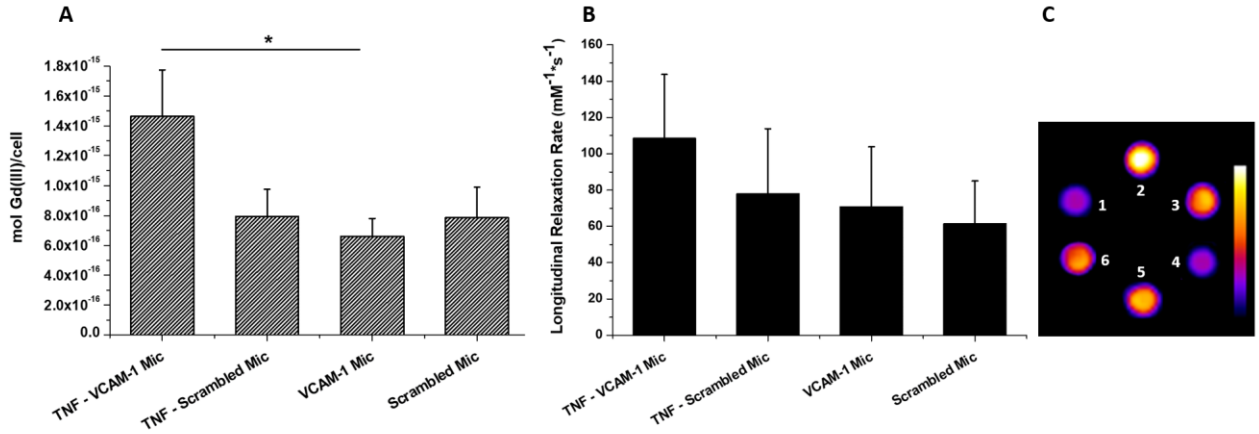

Figure 2. *In vitro* study on targeted or scrambled micelle binding affinity towards VCAM-1 in activated or non-activated brain endothelial cells. A) moles of Gd(III) per cell calculated using Bradford assay, to determine the number of cells, and ICP-MS, to measure Gd(III) concentration. B) r_1 values of bEnd.3 cells measured at 7.0 T and normalized to ICP-MS values of Gd(III) concentration. C) T_{1w} image (pseudo-colorized, originally in gray scale) of 1) activated bEnd.3 cells, 2) activated bEnd.3 cells incubated with VCAM-1 targeted micelles, 3) activated bEnd.3 cells incubated with scrambled micelles, 4) non-activated bEnd.3 cells, 5) non-activated bEnd.3 cells incubated with VCAM-1 targeted micelles and 6) non- activated bEnd.3 cells incubated with scrambled micelles. The incubation was carried out at 4°C (30 min). Error bars represent SE of the mean (* $p < 0.05$).

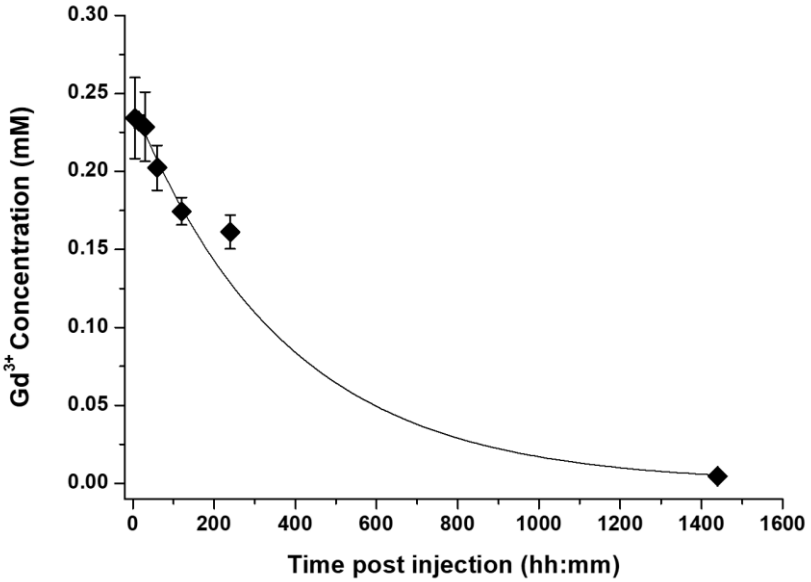

Figure 3. Mean half-life time of VCAM-1 targeted micelles assessed in healthy C57BL/6J female mice (*n*=3) by ICP-MS analysis of blood samples collected at different time points post injection. Error bars represent SE of the mean.

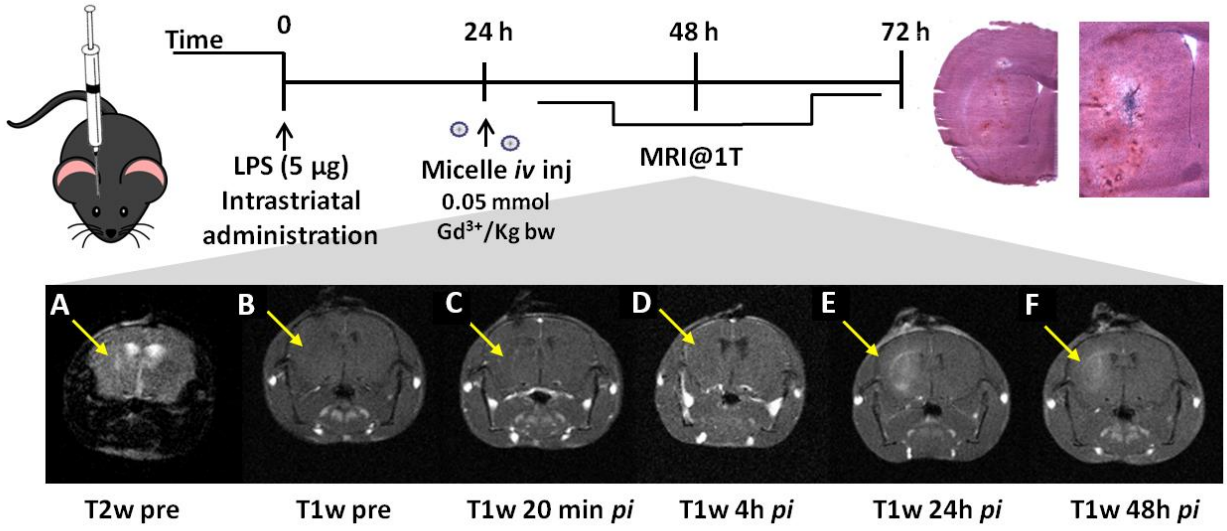

Figure 4. Top) Schematic representation of the experimental procedure: C57BL6/J mice were subjected to surgery to inject 5 µg of LPS intra-striatally in the right hemisphere; 24 h after surgery VCAM-1 targeted micelles were administered intravenously and the mice were imaged at 1 T: A) T_{2w} image pre-injection, B) T_{1w} image pre-injection, C) T_{1w} image 20 min post injection, D) T_{1w} image 4 h post injection, E) T_{1w} image 24 h post injection, F) T_{1w} image 48 h post injection. Yellow arrows indicate the inflamed region.

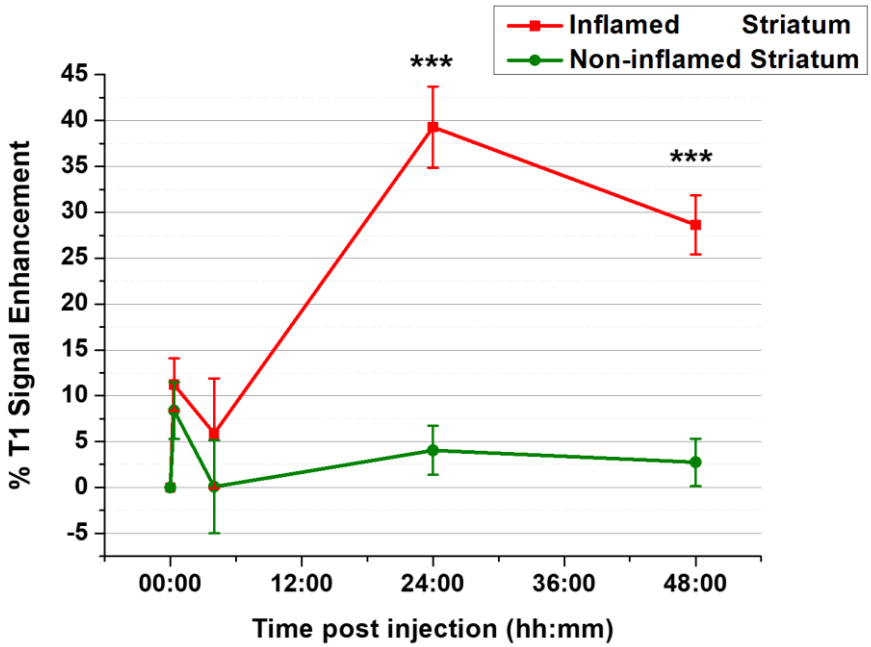

Figure 5. % T_1-SE calculated over pre-images in the striatum at different time points after the injection of VCAM-1 targeted micelles. The nanosystem was administered 24 hours after the induction of inflammation (* p<0.001, n=8). Error bars represent SE of the mean.**

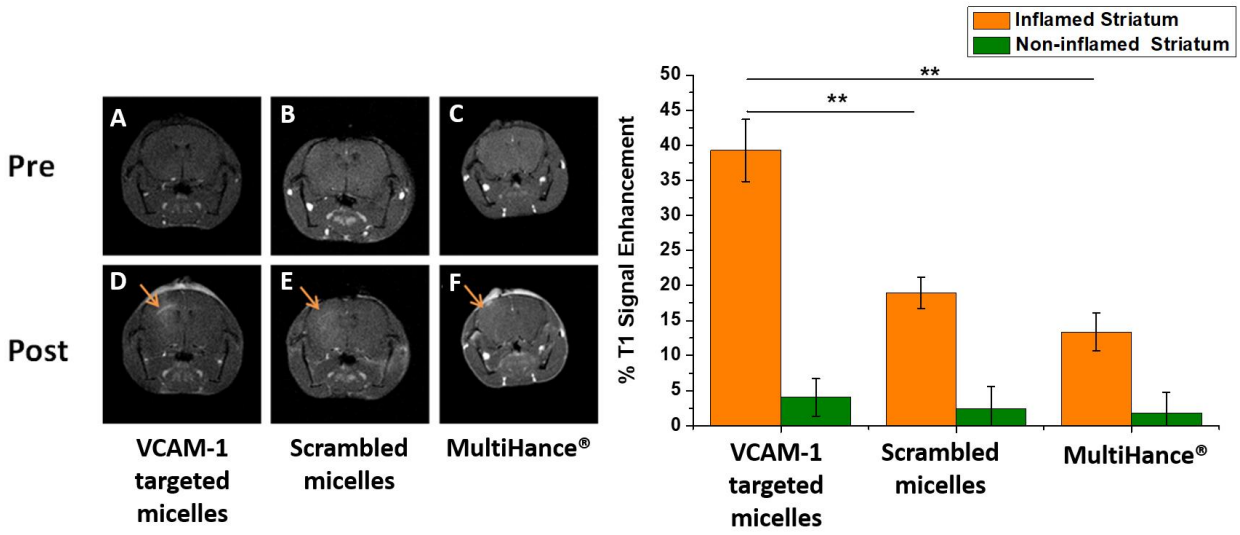

Figure 6. Left: 1T MRI of neuroinflamed mice before and 24h after *iv* injection of (A,D) VCAM-1 targeted or (B,E) scrambled micelles (0.05 $mmol_{Gd3+}$/kg), or 20 min post (C,F) MultiHance (0.2 $mmol_{Gd3+}$/Kg) administration. Right: corresponding % T1 Signal Enhancement calculated in the diseased (orange bars) and healthy (green bars) striatum. Error bars represent SE of the mean. (p<0.01, n=16)**

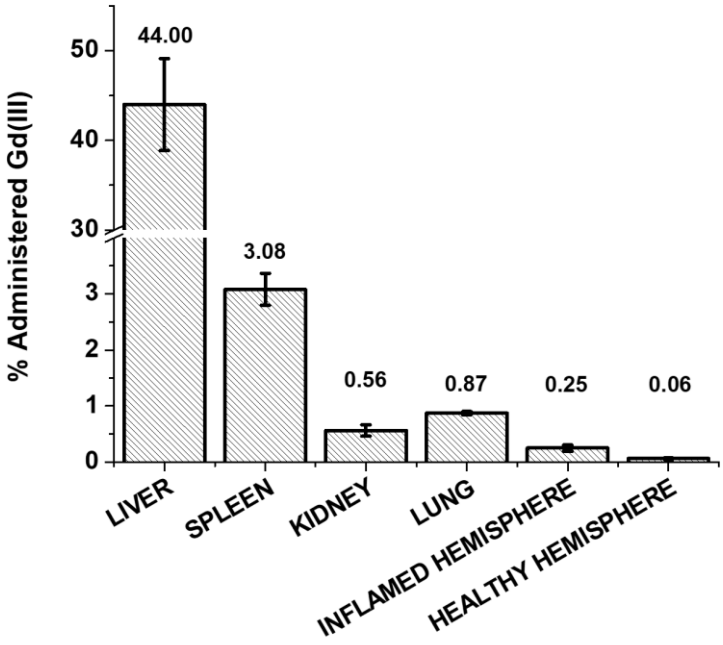

Figure 7. Quantification of % Gd^{3+} content in main excretory and target organs, 24 hours post administration of VCAM-1 targeting micelles (*n*=6), calculated over the total administered Gd^{3+} dosage. The % mean value measured in each organ is displayed in the chart. Error bars represent SE of the mean.

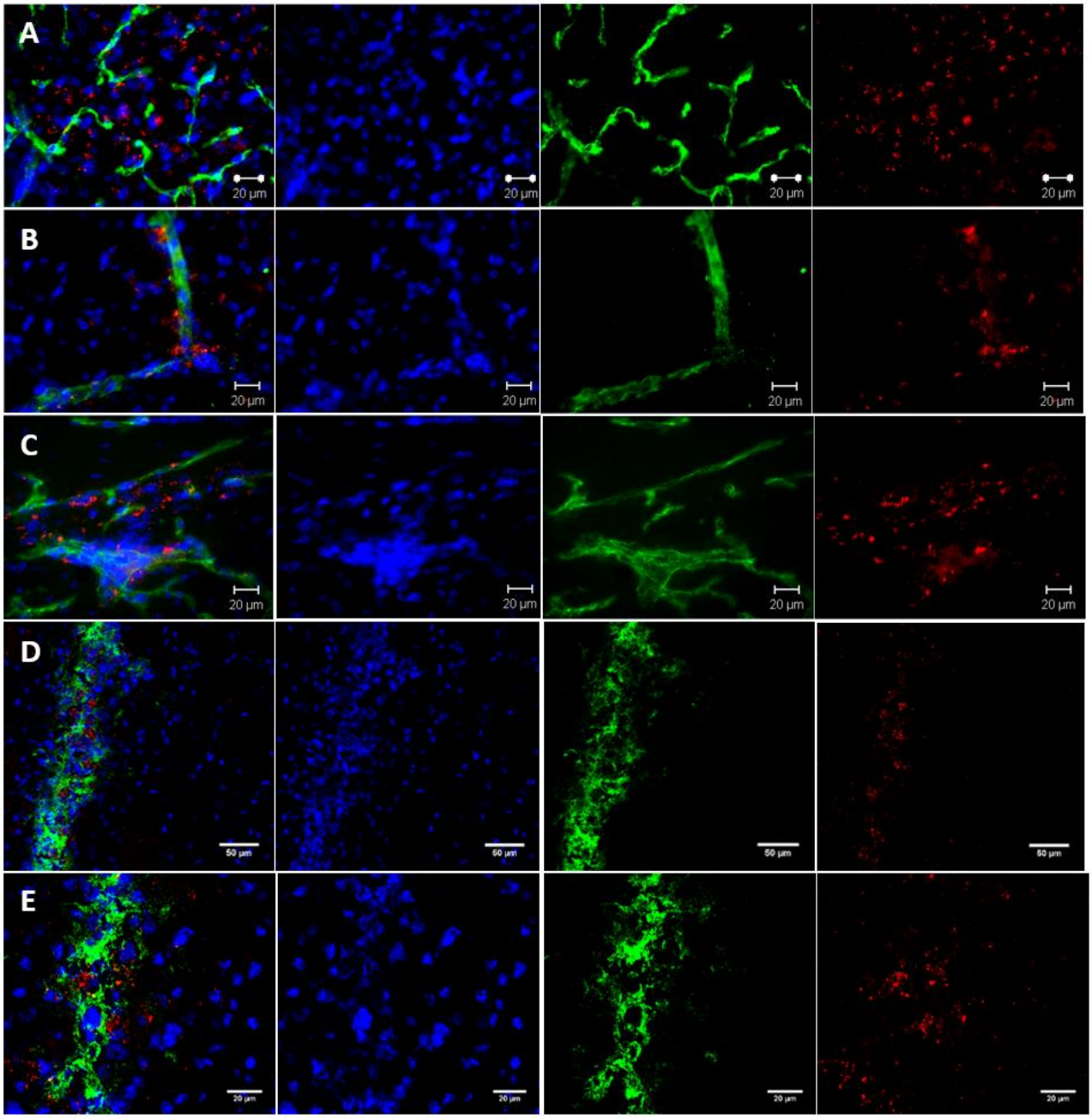

Figure 8. Confocal microscopy images of the inflamed striatum of C57BL/6J mice taken 24 hours post VCAM-1 targeting micelle injection. In the first column merge of the three channels is displayed, in the other columns channels are displayed separately. Nuclei are stained in blue, micelles are shown in red. A) CD31 staining (green) of brain endothelial cells; B-C) VCAM-1 staining (green) showing colocalization of micelles and related target; D-E) macrophage staining with anti F4/80 antibody (green) at two different magnifications.

References

1. Amor S, Puentes F, Baker D, van der Valk P. Inflammation in neurodegenerative diseases. *Immunology*. 2010;**129**(2):154-169.
2. Faden AI, Loane DJ. Chronic Neurodegeneration After Traumatic Brain Injury: Alzheimer Disease, Chronic Traumatic Encephalopathy, or Persistent Neuroinflammation? *Neurotherapeutics*. 2015;**12**(1):143-150.
3. Ellwardt E, Zipp F. Molecular mechanisms linking neuroinflammation and neurodegeneration in MS. *Exp Neurol*. 2014; **262** Pt A:8-17.
4. Ory D, Celen S, Verbruggen A, Bormans G. PET radioligands for in vivo visualization of neuroinflammation. *Curr Pharm Des*. 2014; **20**(37): 5897-913.
5. Jacobs AH, Tavitian B, the INMiND consortium. Noninvasive molecular imaging of neuroinflammation. *Journal of Cerebral Blood Flow & Metabolism*. 2012;**32**(7):1393-1415. doi:10.1038/jcbfm.2012.53.
6. Morales I, Guzmán-Martínez L, Cerda-Troncoso C, Farías GA, Maccioni RB. Neuroinflammation in the pathogenesis of Alzheimer's disease. A rational framework for the search of novel therapeutic approaches. *Frontiers in Cellular Neuroscience*. 2014;**8**:112.
7. Wilcock DM. A Changing Perspective on the Role of Neuroinflammation in Alzheimer's Disease. *International Journal of Alzheimer's Disease*, 2012, **2012**:495243.
8. Quarantelli M. MRI/MRS in neuroinflammation: methodology and applications. *Clinical and Translational Imaging*. 2015;**3**:475-489.
9. Witte ME, Geurts JJ, de Vries HE, van der Valk P, van Horssen J. Mitochondrial dysfunction: A potential link between neuroinflammation and neurodegeneration? *Mitochondrion*, 2010, **10**(5): 411-8.
10. Heneka MT et al. Neuroinflammation in Alzheimer's disease**.** *Lancet Neurol*, 2015, **14**(4):388-405.

11. Frank-Cannon TC, Alto LT, McAlpine FE, Tansey MG. Does neuroinflammation fan the flame in neurodegenerative diseases? *Molecular Neurodegeneration*. 2009;**4**:47. doi:10.1186/1750-1326-4-47.
12. Hirsch EC, Hunot S. Neuroinflammation in Parkinson's disease: a target for neuroprotection? *Lancet Neurol*, 2009, **8**(4):382-97.
13. Haider L, Zrzavy T, Hametner S, et al. The topograpy of demyelination and neurodegeneration in the multiple sclerosis brain. *Brain*. 2016;**139**(3):807-815. doi:10.1093/brain/awv398.
14. Crotti A, Glass CK. The choreography of neuroinflammation in Huntington's disease. *Trends in immunology*. 2015;**36**(6):364-373. doi:10.1016/j.it.2015.04.007.
15. Aronica E, Crino PB. Inflammation in epilepsy: clinical observations. *Epilepsia.* 2011;**52** Suppl 3:26-32.
16. Agrawal M, Biswas A. Molecular diagnostics of neurodegenerative disorders. *Frontiers in Molecular Biosciences*. 2015;**2**:54. doi:10.3389/fmolb.2015.00054.
17. M Mueller SG, Weiner MW, Thal LJ, et al. Ways toward an early diagnosis in Alzheimer's disease: The Alzheimer's Disease Neuroimaging Initiative (ADNI). *Alzheimer's & dementia : the journal of the Alzheimer's Association*. 2005;**1**(1):55-66. doi:10.1016/j.jalz.2005.06.003.
18. Stoessl AJ. Neuroimaging in the early diagnosis of neurodegenerative disease. *Translational Neurodegeneration*. 2012;**1**:5. doi:10.1186/2047-9158-1-5.
19. Landau SM, Fero A, Baker SL, et al. Measurement of Longitudinal β-Amyloid Change with ^{18}F-Florbetapir PET and Standardized Uptake Value Ratios. *Journal of nuclear medicine : official publication, Society of Nuclear Medicine*. 2015;**56**(4):567-574. doi:10.2967/jnumed.114.148981.
20. Shoghi-Jadid K, Small GW, Agdeppa ED, Kepe V, Ercoli LM, Siddarth P, Read S, Satyamurthy N, Petric A, Huang SC, Barrio JR. Localization of neurofibrillary tangles and

beta-amyloid plaques in the brains of living patients with Alzheimer disease. *Am J Geriatr Psychiatry*. 2002;**10**(1):24-35.

21. Rupprecht R, Papadopoulos V, Rammes G, Baghai TC, Fan J, Akula N, Groyer G, Adams D, Schumacher M. Translocator protein (18 kDa) (TSPO) as a therapeutic target for neurological and psychiatric disorders. *Nat Rev Drug Discov*, 2010, **9**:971–988.
22. Venneti S, Lopresti BJ, Wiley CA. Molecular imaging of microglia/macrophages in the brain. *Glia*. 2013;**61**(1):10-23. doi:10.1002/glia.22357.
23. Thiel A, Heiss WD. Imaging of microglia activation in stroke. *Stroke*, 2011, **42**(2):507-12.
24. Chauveau F, Boutin H, Van Camp N, Dolle F, Tavitian B. Nuclear imaging of neuroinflammation: a comprehensive review of [11C]PK11195 challengers. *Eur J Nucl Med Mol Imaging*, 2008, **35**:2304–2319.
25. Jalbert JJ, Daiello LA, Lapane KL. Dementia of the Alzheimer type. *Epidemiol Rev.* 2008, **30**:15-34.
26. Sabuncu MR, Desikan RS, Sepulcre J, et al. The Dynamics of Cortical and Hippocampal Atrophy in Alzheimer Disease. *Archives of neurology*. 2011;**68**(8):1040-1048. doi:10.1001/archneurol.2011.167.
27. Mascalchi M, Lolli F, Della Nave R, Tessa C, Petralli R, Gavazzi C, Politi LS, Macucci M, Filippi M, Piacentini S. Huntington disease: volumetric, diffusion-weighted, and magnetization transfer MR imaging of brain. *Radiology*. 2004; **232**(3):867-73.
28. Filippi M, Rocca MA. MR imaging of multiple sclerosis. *Radiology*, 2011, **259**(3):659-81.
29. Ge Y. Multiple sclerosis: the role of MR imaging. *AJNR Am J Neuroradiol*, 2006, **27**(6):1165-76.
30. Tuite PJ, Mangia S, Michaeli S. Magnetic Resonance Imaging (MRI) in Parkinson's Disease. *Journal of Alzheimer's disease & Parkinsonism*. **2013**;Suppl 1:001-. doi:10.4172/2161-0460.S1-001.

31. Schwarz ST, Afzal M, Morgan PS, Bajaj N, Gowland PA, et al. The 'Swallow Tail' Appearance of the Healthy Nigrosome – A New Accurate Test of Parkinson's Disease: A Case-Control and Retrospective Cross-Sectional MRI Study at 3T. *PLOS ONE,* 2014; **9**(4): e93814.
32. Ransohoff RM, Kivisäkk P, Kidd K. Three or more routes for leukocyte migration into the central nervous system. *Nat Rev Immunol.* 2003, **3**(7):569-81.
33. Wilson EH, Weninger W, Hunter CA. Trafficking of immune cells in the central nervous system. *The Journal of Clinical Investigation*. 2010;**120**(5):1368-1379. doi:10.1172/JCI41911.
34. Ceulemans A-G, Zgavc T, Kooijman R, Hachimi-Idrissi S, Sarre S, Michotte Y. The dual role of the neuroinflammatory response after ischemic stroke: modulatory effects of hypothermia. *Journal of Neuroinflammation*. 2010;**7**:74. doi:10.1186/1742-2094-7-74.
35. Ferretti MT, Merlini M, Späni C, Gericke C, Schweizer N, Enzmann G, Engelhardt B, Kulic L, Suter T, Nitsch RM. T-cell brain infiltration and immature antigen-presenting cells in transgenic models of Alzheimer's disease-like cerebral amyloidosis. *Brain Behav Immun.* 2016; **54**:211-25.
36. Man S, Ubogu EE, Ransohoff RM. Inflammatory cell migration into the central nervous system: a few new twists on an old tale. *Brain Pathol.* 2007; **17**(2):243-50.
37. McAteer MA, Sibson NR, von zur Mühlen C, et al. *In vivo* magnetic resonance imaging of acute brain inflammation using microparticles of iron oxide. *Nature medicine*. 2007;**13**(10):1253-1258. doi:10.1038/nm1631.
38. McAteer MA, Akhtar AM, von zur Muhlen C, Choudhury RP. An approach to molecular imaging of atherosclerosis, thrombosis, and vascular inflammation using microparticles of iron oxide. *Atherosclerosis*. 2010;209(1):**18**-27. doi:10.1016/j.atherosclerosis.2009.10.009.
39. Burtea C, Ballet S, Laurent S, Rousseaux O, Dencausse A, Gonzalez W, Port M, Corot C, Vander Elst L, Muller RN. Development of a magnetic resonance imaging protocol for the

characterization of atherosclerotic plaque by using vascular cell adhesion molecule-1 and apoptosis-targeted ultrasmall superparamagnetic iron oxide derivatives. *Arterioscler Thromb Vasc Biol*. 2012;**32**(6):e36-48. doi: 10.1161/ATVBAHA.112.245415.

40. Burtea C, Laurent S, Port M, Lancelot E, Ballet S, Rousseaux O, Toubeau G, Vander Elst L, Corot C, Muller RN. Magnetic resonance molecular imaging of vascular cell adhesion molecule-1 expression in inflammatory lesions using a peptide-vectorized paramagnetic imaging probe. *J Med Chem.* 2009;**52**(15):4725-42. doi: 10.1021/jm9002654.
41. Zimny A, Neska-Matuszewska M, Bladowska J, Sąsiadek MJ. Intracranial Lesions with Low Signal Intensity on T2-weighted MR Images – Review of Pathologies. *Polish Journal of Radiology*. 2015;**80**:40-50. doi:10.12659/PJR.892146.
42. Pagoto A, Stefania R, Garello F, Arena F, Digilio G, Aime S, Terreno E. Paramagnetic Phospholipid-Based Micelles Targeting VCAM-1 Receptors for MRI Visualization of Inflammation. *Bioconjug Chem*. 2016; **27**(8):1921-30.
43. Vaccaro M, Mangiapia G, Paduano L, Gianolio E, Accardo A, Tesauro D, Morelli G. Structural and relaxometric characterization of peptide aggregates containing gadolinium complexes as potential selective contrast agents in MRI. *ChemPhysChem,* 2007, **8**:2526– 38.
44. Körbelin J, Dogbevia G, Michelfelder S, et al. A brain microvasculature endothelial cell-specific viral vector with the potential to treat neurovascular and neurological diseases. *EMBO Molecular Medicine*. 2016;**8**(6):609-625. doi:10.15252/emmm.201506078.
45. Hohlfeld R, Kerschensteiner M, Meinl E. Dual role of inflammation in CNS disease. *Neurology*. 2007;**68**(22 Suppl 3):S58-63; discussion S91-6.
46. Pulli B, Chen JW. Imaging Neuroinflammation – from Bench to Bedside. *Journal of clinical & cellular immunology*. 2014;**5**:226. doi:10.4172/2155-9899.1000226.
47. Hoyte LC, Brooks KJ, Nagel S, et al. Molecular magnetic resonance imaging of acute vascular cell adhesion molecule-1 expression in a mouse model of cerebral ischemia. *Journal of*

Cerebral Blood Flow and Metabolism: Official Journal of the International Society of Cerebral Blood Flow and Metabolism. 2010;**30**(6):1178-1187. doi:10.1038/jcbfm.2009.287.

48. Serres S, Soto MS, Hamilton A, et al. Molecular MRI enables early and sensitive detection of brain metastases. *Proc Natl Acad Sci USA*, 2012, **109**:6674–6679.
49. Chen JW, Breckwoldt MO, Aikawa E, Chiang G, Weissleder R. Myeloperoxidase-targeted imaging of active inflammatory lesions in murine experimental autoimmune encephalomyelitis. *Brain : a journal of neurology*. 2008;**131**(4):1123-1133.
50. Sipkins DA, Gijbels K, Tropper FD, Bednarski M, Li KC, Steinman L. ICAM-1 expression in autoimmune encephalitis visualized using magnetic resonance imaging. *J Neuroimmunol.* 2000;**104**(1):1-9.
51. Wuerfel E, Infante-Duarte C, Glumm R, Wuerfel JT. Gadofluorine M-enhanced MRI shows involvement of *circumventricular organs in neuroinflammation. Journal of Neuroinflammation. 2010; 7*:70.
52. Chung EJ, Cheng Y, Morshed R, et al. Fibrin-binding, peptide amphiphile micelles for targeting glioblastoma. *Biomaterials*. 2014;**35**(4):1249-1256.
53. Jokerst JV, Lobovkina T, Zare RN, Gambhir SS. Nanoparticle PEGylation for imaging and therapy. *Nanomedicine (London, England)*. 2011;**6**(4):715-728. doi:10.2217/nnm.11.19.
54. Wilhelm S et al. Analysis of nanoparticle delivery to tumours. *Nature Reviews Materials*, 2016, **1**(5):16014. doi:10.1038/natrevmats.2016.14
55. Dietrich T et al. Pre-saturation of the liver and subsequent administration of the contrast agent. WO Pat., 2015044312 A1, 2016.
56. Kedar U, Phutane P, Shidhaye S, Kadam V. Advances in polymeric micelles for drug delivery and tumor targeting. *Nanomedicine*. 2010;**6**(6):714-29. doi: 10.1016/j.nano.2010.05.005.
57. Al-Achi A, Jonathan Lawrence BS. Micelles: Chemotherapeutic Drug Delivery. *Clin Pharmacol Biopharm*, 2013, **2**:e114.

58. Gaucher G, Satturwar P, Jones MC, Furtos A, Leroux JC. Polymeric micelles for oral drug delivery. *Eur J Pharm Biopharm*. 2010;**76**(2):147-58. doi: 10.1016/j.ejpb.2010.06.007.